Influence of vanadium on optical and mechanical properties of aluminosilicate glasses

Maria Rita Cicconi, Zhuorui Lu, Tobias Uesbeck, Leo van Wüllen, Delia S. Brauer, Dominique de Ligny

Angaben zur Veröffentlichung / Publication details:

Cicconi, Maria Rita, Zhuorui Lu, Tobias Uesbeck, Leo van Wüllen, Delia S. Brauer, and Dominique de Ligny. 2020. "Influence of vanadium on optical and mechanical properties of aluminosilicate glasses." *Frontiers in Materials* 7 (June): 161. https://doi.org/10.3389/fmats.2020.00161.

frontiers in Materials

ORIGINAL RESEARCH
published: 24 June 2020
doi: 10.3389/fmats.2020.00161

Influence of Vanadium on Optical and Mechanical Properties of Aluminosilicate Glasses

Maria Rita Cicconi[1], Zhuorui Lu[1†], Tobias Uesbeck[1,2], Leo van Wüllen[2], Delia S. Brauer[3] and Dominique de Ligny[1]*

[1] Lehrstuhl für Glas und Keramik, Department Werkstoffwissenschaften, FAU Erlangen-Nürnberg, Erlangen, Germany, [2] Institut für Physik, Universität Augsburg, Augsburg, Germany, [3] Otto Schott Institute of Materials Research, Friedrich Schiller University, Jena, Germany

OPEN ACCESS

Edited by:
Jürgen Horbach,
Heinrich Heine University of Düsseldorf, Germany

Reviewed by:
Sylwester Janusz Rzoska,
Institute of High Pressure Physics (PAN), Poland
Chao Liu,
Wuhan University of Technology, China

***Correspondence:**
Maria Rita Cicconi
maria.rita.cicconi@fau.de

†Present address:
Zhuorui Lu,
Institut de Physique de Nice, Université Côte d'Azur, Nice, France

Specialty section:
This article was submitted to Ceramics and Glass, a section of the journal Frontiers in Materials

Received: 20 March 2020
Accepted: 04 May 2020
Published: 24 June 2020

Citation:
Cicconi MR, Lu Z, Uesbeck T, van Wüllen L, Brauer DS and de Ligny D (2020) Influence of Vanadium on Optical and Mechanical Properties of Aluminosilicate Glasses. Front. Mater. 7:161. doi: 10.3389/fmats.2020.00161

V_2O_5 was introduced up to 9 wt.% in a peralkaline alkaline earth aluminosilicate glass and up to 4.8 wt.% in two sodo aluminosilicate glasses, respectively, a peralkaline and a peraluminous one. This introduction had a strong effect on thermal properties, and in particular, on glass transition and crystallization temperatures of the peraluminous glass, which dropped by 89 K, while a moderate drop of ∼20 K was observed for the two other glasses. Still, the glass stability and the glass-forming ability stayed almost unmodified. The elastic properties measured by Brillouin spectroscopy show a decrease with added Vanadium for the depolymerized alkali earth aluminosilicate and the peraluminous sodo aluminosilicate. In contrast, the elastic properties remained unchanged for the peralkaline composition. Using optical absorption, the proportion of V^{5+}, which is largely dominant, was found to follow the trend predicted using optical basicity considerations. A large photoluminescence emission, centered at ∼560 nm, was found for all glasses, upon excitation in the UV edge at both ∼280 and ∼350 nm. The emission band positions were relatively insensitive to the glass composition, whereas their intensities show variations of one order of magnitude between the sodium peralkaline composition and the calcium depolymerized glass. A too-high concentration of V_2O_5 shows a quenching effect on the emission. Polarized and cross-polarized Raman spectroscopy allowed us to identify the different environments around the $V^{5+}O_4$ tetrahedra. The highly polarizable $V^{5+}O_4$ tetrahedra associated with two non-bridging oxygens, vibrating at 860 cm^{-1}, is proposed to be responsible for the more efficient charge transfer. At the opposite end, the formation of VO_4-AlO_4 units is proposed to quench luminescence properties. Furthermore, we observed that, upon thermal treatment, the optical properties of the glasses are significantly modified without observable structural modifications or evolution of the elastic properties.

Keywords: thermal treatment, redox, cation speciation, optical absorption, glass structure changes, thermal history

INTRODUCTION

Vanadium is a transition element that in glasses can be stable with different speciation. This means that depending on synthesis conditions, bulk chemistry, and total V amount, vanadium ions might be stabilized with oxidation states ranging from the oxidized V^{5+} to V^{4+} to the reduced V^{3+}, each albeit with a different favorite oxygen bonding environment (coordination, bond type) (Johnston, 1965a,b; Schreiber, 1986; Leister et al., 1999). Among the different species, based on cation field strength (CFS) considerations (Dietzel, 1948), vanadium ions can enter in the amorphous network with different roles, namely network formers, modifiers or intermediated. Indeed, both penta- and tetravalent V species could be found in 4-fold coordination ($^{[4]}V^{5+}$, $^{[4]}V^{4+}$) with the $V^{5+}O_4$ tetrahedra having a V = O apex, but also with higher coordination environments, such as tetragonal pyramid ($^{[5]}V^{4+}$) or octahedral coordination (e.g., $^{[6]}V^{5+}$) (Anpo et al., 1980; Dzwigaj et al., 2000; Giuli et al., 2004; Kniec and Marciniak, 2019).

The bulk chemistry is one of the main factors influencing multivalent cation speciation (e.g., for iron, and cerium Mysen and Richet, 2005; Cicconi et al., 2015, 2017), and studies on the influence of chemistry on optical, physical, and mechanical properties of V-doped glasses are surprisingly scarce. This lack of information hampers the possibility of finding applications for this versatile cation. It is important to point out that changes in cation speciation might influence the overall properties of the host glass, and in particular, the physical and optical properties. The latter is particularly important, because changes only limited in the V average redox ratio already can provide a variety of responses in terms of optical properties (electronic configuration varies from $3d^0$ to $3d^2$; e.g., Johnston, 1965a; Anpo et al., 1980; Dzwigaj et al., 2000). And indeed, the color associated with V-bearing glasses usually hampers their use for, e.g., optical applications where colorless transparent materials are required. On the other hand, the several bands achievable in the UV-Vis-NIR regions make this element intriguing for other uses, such as in the case of luminescence nanothermometry, or tunable phosphorous (Gao et al., 2011; Kniec and Marciniak, 2019 and references therein).

Besides the optical properties, V can act as network former cation in glasses, forming the $V^{5+}O_4$ tetrahedral species, similarly to the more famous P^{5+} ions. Like phosphorous, vanadium might have some preferred associations (Na, Fe, or Al for example) in the glass network that influence the network connectivity (Mysen, 1992; Toplis and Dingwell, 1996; Cody et al., 2001; Mysen and Richet, 2005). Furthermore, since vanadium is a transition element, the electronic energy levels are strongly dependent on bond strength, coordination, and kind of first neighbors. Thus, to attain a deep understanding of the correlation between atomic structure and macroscopic properties, a fundamental study of the influence of bulk chemistry and thermal history is required.

With that in mind, we investigated different glasses, either alkali-free or alkali-bearing, and doped them with vanadium up to ∼9 wt.% with the aim of shedding some light on the influence of (i) synthesis conditions, (ii) bulk chemistry, and (iii) thermal history on vanadium speciation and the optical and structural properties of the host glasses.

Alkali-free aluminosilicate glasses and glass-ceramics in the system CaO-MgO-Al_2O_3-SiO_2 are interesting for many applications, because of their dielectric properties and high mechanical and chemical resistance (Shelby, 1985; Toya et al., 2004; Khater, 2010). Here, we selected the Diopside-Anorthite binary system that has a very good glass ability at the eutectic point (1,274°C). For the alkali-bearing glasses, the ternary system Na_2O-Al_2O_3-SiO_2 (NAS) was selected. Sodium in NAS systems acts either as a charge compensator for Al or as a network modifier. In the former case, it influences the local structure and coordination number of Al, whereas in the latter case, it produces non-bridging oxygens. Therefore, in peralkaline composition (Al/Na < 1), Al is mainly in $[AlO_4]$-Na structure since there are enough alkali cations to balance the charge, whereas in peraluminous compositions (Al/Na > 1) aluminum can be easily found in higher coordination (McKeown et al., 1984; Neuville and Mysen, 1996; Xiang et al., 2013).

Glasses were synthetized in air by melt quenching, and portions of the glasses were also thermally treated at a temperature just above Tg for different times. Glasses were investigated at different scale-lengths with various techniques: photoluminescence, optical absorption, and Raman spectroscopy, and mechanical properties were probed by using Brillouin spectroscopy. We verified that the chemistry has a strong influence on the initial vanadium speciation and that the glass thermal properties are affected by vanadium incorporation. Interestingly, we determined that the speciation of vanadium is strongly correlated to the kind of neighbors in the second coordination shell and that variation in the photoluminescence excitation can be associated with the vanadium species observed via Raman spectroscopy. Ergo, variations on the bond strength, oxygen-bonding environment and kind of second neighbors can be correlated (and possibly controlled) when looking in details at the network connectivity.

MATERIALS AND METHODS

Glass Syntheses, Thermal Treatments

Glasses are either in the quaternary system CaO-MgO-Al_2O_3-SiO_2 or in ternary system Na_2O-Al_2O_3-SiO_2, in order to study, respectively, alkali-free and alkali-bearing compositions. Diopside-Anorthite (DiAn) at the eutectic compositions (50 mol% each) have been synthesized starting from dried oxides and carbonated weighed in stoichiometric proportions. The mixed powders were decarbonized at 830°C overnight and then melted in Pt-Rd crucible at 1,450°C for 3 h in air. The melt was cast at room temperature on a brass plate. The obtained glass was finely crushed and melted again in the same conditions. Finally, the homogeneous bubble-free melt was cast in a brass mold and annealed at 600°C, a temperature below their glass transition temperatures (see **Table 1**). A portion of the pristine DiAn glass was finely crushed and doped with different amounts of V_2O_5 (5 wt.% and 10 wt.%). Vanadium-doped samples are labeled DiAn5V and DiAn10V and contain, respectively, 1.7 and 3.5

TABLE 1 | Percentage of mass determined by ICP analysis (wt.%) and the recalculated mol% of the investigated glasses.

Sample	SiO_2	Al_2O_3	MgO	CaO	Na_2O	V_2O_5	V_2O_5 ICP wt%	Density (g/cm^3)	Vm (cm^3/mol)	n_D	Tg (°C)	Tx (°C)	Tm (°C)	Λ
DiAn (wt%)	50.2	15.3	10.6	23.1										
mol%	50.4	9.0	15.8	24.8				2.785 (17)	21.43 (13)	1.593 (0)	742	968, 1,071	1,276	0.60
DiAn5V mol%	49.3	8.9	15.8	24.7		1.3	4.0	2.788 (7)	21.99 (5)	1.609 (0)	728	948, 1,044	1,240	0.60
DiAn10V mol%	48.3	8.7	15.4	24.1		3.5	9.9	2.789 (4)	22.93 (3)	1.621 (0)	703	926, 1,026	1,200	0.61
NA66.10 (wt%)	61.5	16.0			21.9		0							
mol%	66.8	10.2			23.1			2.457 (6)	26.34 (6)	1.501 (1)	523	867		0.58
NAV66.10 mol%	65.5	9.8			22.9	1.8	4.8	2.473 (5)	27.00 (5)	1.522 (2)	514	850		0.59
NA66.18 (wt%)	58.2	27.1			14.0		0							
mol%	66.4	18.2			15.5			2.426 (10)	27.99 (11)	1.504 (3)	814			0.56
NAV66.18 mol%	65.5	17.7			15.0	1.9	4.8	2.432 (9)	28.81 (10)	1.515 (1)	725	1,116		0.57

Section Analytical Methods reports details of the theoretical optical basicity (Λ) calculations.

mol% of V_2O_5. DiAn10V samples were melted at 1,450°C for 4 h and cast at the same condition as the pristine DiAn composition.

The second glass system selected is the alkali-bearing NAS system (Na_2O-Al_2O_3-SiO_2). Two glass compositions, containing different Al amounts, were selected. Indeed, the Al/alkali (Na) ratio was varied, while keeping constant the SiO_2 content, to obtain a peralkaline (Al < alkali) and a peraluminous glass (Al > alkali). The glass stoichiometry is 66 mol% SiO_2-(16.33, 23.33) mol% Na_2O–(18, 10) mol% Al_2O_3. The pristine materials were melted in air at 1,400°C for 2 h, and after quenching and crushing, they were remelted again at 1,500°C for 2 h. The homogeneous melts were fast-quenched by dipping the crucible bottom in water. Portions of the pristine glasses were finely grounded and doped with 5 wt.% vanadium oxide (V_2O_5), then melted and cast under the same conditions used for the pristine glasses. V-free pristine glasses are named NA66.y, with $y = Al_2O_3$ and $Na_2O = 100 - (66 + y)$. V-bearing aluminosilicate glasses are labeled NAV66.y.

Analysis of the base glass compositions was obtained by ICP-MS and are reported in **Table 1**. The molar concentrations were obtained by the renormalization of the weight composition to 100%. Very good agreement is found between the analyzed and nominal compositions of the pristine glasses. For the glass with added V_2O_5, only the Vanadium content was analyzed by ICP-MS. The molar composition was deduced from the measurement of the base glass, taking into account the analyzed amount of V_2O_5. Since the V_2O_5 amount present in the glass is lower than the targeted amount, it is suggested that some volatilization of V occurred during the melting.

Small glasses pieces were double-polished to optical quality with SiC paper until 5 μm and with diamond suspension until 1 μm. Polished samples were used for thermal treatments as well, to reduce surface tension and to avoid induced crystallization. Thermal treatments of all glasses were done in small furnaces with a secondary thermocouple placed directly in contact with the sample edge, to minimize temperature errors. Thermal treated samples are labeled "*samplename*" TT"*x*d" with *x* representing the time (days): e.g., DiAn5VTT3d represents the diopside-anorthite glass doped with 5 wt.% V_2O_5 and thermally treated for 3 days. Thermal treatments have been done for different times and the sample list is reported in **Table 2**, along with glass properties. In the case of DiAn10V, partial crystallization was observed after 3 days at 760°C. Therefore, further heat treatments were done closer to Tg at 735°C.

Analytical Methods

Density was measured by the Archimedes method with water. An average of three to four measurements were done for each sample. The molar volume of the glasses has been calculated according to $V_m = \sum \frac{n_i M_i}{\rho}$, where *n* and *M* are, respectively, the molar fraction and the molecular weight of the oxide *i*, and ρ the glass density. The Refractive Index *n* at the Na-D line and the Abbe number of the polished samples have been measured on an Abbe refractometer. The monobromonapthalene was used as the contact layer between the sample and prism of the refractometer. Thermal properties, i.e. glass transition, the onset of crystallization, and melting temperature, were measured from differential scanning calorimetry (DSC, NETZSCH DSC 404F1) at a constant heating and cooling rate (20 K/min) for DiAn system. For the NAS system, the heating and cooling rates used were, respectively, 30 and 20 K/min.

Absorption spectra were measured using a UV-VIS spectrometer (Lambda 950, Perkin Elmer). All measurements were carried out on polished glasses in the range 1,400 to

TABLE 2 | Thermal treatment (TT) parameters and properties.

Label	TT Temperature (°C)	Time	ΔT (°C)	ρ (g/cm^3)	n_D (error < 0.002)	Abbe
DiAn				2.785 (17)	1.593 (2)	56 (2)
DiAnTT0.5h	774	0.5 h	32	2.786 (5)	1.592	51
DiAnTT1d	774	1 day	32	2.788 (3)	1.598 (9)	57 (1)
DiAnTT3d	774	3 days	32	2.773 (1)		
DiAn5V				2.788 (7)	1.609	47 (3)
DiAn5VTT0.5h	760	0.5 h	32	2.793 (64)		
DiAn5VTT1d	760	1 day	32	2.797 (22)	1.610 (1)	49 (1)
DiAn5VTT3d	760	3 days	32	2.798 (3)	1.607 (1)	47 (1)
DiAn5VTT7d	760	7 days	32	2.800 (7)	1.609	
DiAn5VTT28d	760	28 days	32	2.801 (7)	1.610	
DiAn10V				2.789 (4)	1.621	45 (3)
DiAn10VTT3d760	760	3 days [§]	57			
DiAn10VTT0.5h	735	0.5 h	32	2.797 (27)		
DiAn10VTT1d	735	1 day	32	2.782 (18)		
DiAn10VTT3d	735	3 days	32	2.815 (30)		
DiAn10VTT7d	735	7 days [§]	32	–		
NA66.10				2.457 (6)	1.501 (1)	48 (2)
NA66.10TT3d	555	3 days	32	2.467 (15)	1.502	50 (1)
NA66.10TT7d	555	7 days	32	2.468 (8)	1.506 (1)	52 (1)
NAV66.10				2.473 (5)	1.522 (2)	50
NAV66.10TT3d	546	3 days	32	2.477 (39)	1.521	
NAV66.10TT7d	546	7 days	32	2.486 (11)	1.523	
NA66.18				2.426 (10)	1.504 (3)	60 (2)
NA66.18TT3d	846	3 days	32	2.428 (5)	1.506 (4)	52 (11)
NA66.18TT7d	846	7 days	32	2.424 (3)	1.509	66
NAV66.18				2.432 (9)	1.515 (1)	
NAV66.18TT3d	757	3 days	32	2.435 (16)	1.517 (1)	61
NAV66.18TT7d	757	7 days	32	2.435 (30)	1.517 (1)	61

[§] *The difference between TT temperature and glass transition temperature ΔT, and properties are reported.*
[§] *sample shows partial surface crystallization upon thermal treatment.*

190 nm. In order to avoid artifacts due to the different lamps and detectors, the spectra were collected in three regions, with overlaps of at least 20 nm in between: e.g., 1,400–850 nm, 870–320 nm, and 340–190 nm. Optical emission and excitation spectra (PL) were collected with a spectrofluorometer equipped with double monochromators (Czerny-Turner) in excitation and emission (Fluorolog3, Horiba Jobin Yvon), using a 450 W Xe-lamp as the excitation source (excitation and emission spectral resolution $\leq$ 2 nm). Raman and Brillouin signals have been acquired simultaneously by using the integrated device ARABICA (for details, see Veber et al., 2018). Raman spectra have been collected with a coherent Sapphire single-frequency 488-nm laser (100 mW) as the excitation source and an iHR 320 Horiba monochromator, combined with a Sincerity UV-VIS CCD camera (grating 1,800 gr/mm), in the frequency range of 10 to 1,500 cm^{-1}. The laser was focused on the sample (polished to optical quality) with a microscope (50× objective) and the backscattering signal was collected. Integrated to the 488 nm excitation laser and Horiba Raman spectrometer, there was a Tandem Fabry-Perot interferometer TFP-2 used to collect the Brillouin signal (Veber et al., 2018). Brillouin back scattering data are collected at a scan amplitude of 475 nm (or 449 nm), a 2.5 mm mirror spacing, 450 entrance pinhole, and 700 detector pinholes. Measurements in platelet geometry were done with 5 mm mirror spacing, 450 entrance pinholes, and 700 detector pinholes. Raman data treatment has been carried out with Horiba software Labspec®. Signals have been background–subtracted with a polynomial function and normalized to the total area. Raman spectra have been also acquired in parallel polarized (VV) and cross-polarized (VH) modes.

RESULTS AND DISCUSSION

Glass Chemistry, V Redox State, and Optical Basicity

Glass compositions have been obtained by ICP-MS analysis and are reported in **Table 1**, along with the recalculated mol%. The three glass series studied, even if very different, can be compared using the concept of optical basicity (Λ) developed by Duffy (1996) and references therein. The optical basicity is the mean

magnitude of negative charge carried by the oxygen atoms and is then sensitive to the strength ionic field of the cations to which it is associated (see e.g., Moretti, 2005). It can be calculated according to $\Lambda = \sum_i X_i \times \Lambda_i$, where X_i is the oxide molar fraction, and Λ_i is the theoretical optical basicity of the oxides ($\Lambda CaO = 1.0$, $\Lambda Na_2O = 1.15$, $\Lambda SiO_2 = 0.48$, $\Lambda MgO = 0.78$, $\Lambda Al_2O_3 = 0.6$ (Duffy, 1993). For the ΛV_2O_5, Duffy (1996) proposed a value of 1.04, though we used here the value of 0.65 reported by Lebouteiller and Courtine (1998) and Hamnabard et al. (2012). It can be noticed from the calculated values in **Table 1** that, for our glasses, V content has only a slight effect on the total optical basicity. A general trend of decreasing optical basicity is then given in the order DiAn, NA66.10, NA66.18. Indeed, even if the non-alkali cations have a stronger charge, DiAn composition has a globally lower optical basicity due to its lower silica content. This optical basicity is in the same order as the trend in regards to the bridging oxygen (BO) concentration. From **Table 1**, it can be easily calculated that DiAn contains 68% of BO and that NA66.10, which is peralkaline, has 86% of BO. Since NA66.18 is peraluminous, it is assumed to contain only BO, considering that higher coordinated Al species still act as network formers. All the results will be always discussed further in this order: DiAn, NA66.10, and NA66.18.

V can be stabilized in three possible valences: V^{5+}, V^{4+}, and V^{3+}. It is possible to describe vanadium in glasses according to the two following equilibria (Johnston, 1965a,b):

$$2O^{2-} + 4V^{5+} \leftrightarrow 4V^{4+} + O_2 \quad (1)$$

$$2O^{2-} + 4V^{4+} \leftrightarrow 4V^{3+} + O_2 \quad (2)$$

The optical basicity approach provided also a way to estimate the redox equilibrium of vanadium ions. The ratio V^{4+}/V^{5+} can be calculated by the empirical equation first proposed by Duffy (1993) and later revised by Farah (2008) for aluminosilicates melts of lime or sodium at 1,325°C:

$$\log\left[\frac{V^{4+}}{V^{5+}}\right] = 3.75 - 8.09\Lambda \quad (3)$$

The predicted V^{4+}/V^{5+} ratios are reported in **Table 3**. This ratio should stay relatively insensitive to the total vanadium content as observed by Farah and Brungs (2003), and V^{5+} should be the predominant species (> 86%) in all glasses. DiAn composition is in agreement with experimental data previously reported (Giuli et al., 2004) and with molecular dynamic simulations (Ori et al., 2011). Similarly, in the NAS ternary system, according to Leister et al. (1999), Al-free sodium silicate glasses, synthesized in air, should have ∼96% of V^{5+}. It can also be noticed that glass polymerization increases the number of reduced species, in agreement with the optical basicity concept. V-doped glasses in this study, depending on the presence of alkali earth cation or the Al/Na molar ratio, have distinct colors, highlighting the stabilization of different V oxidation states depending on composition (see **Figure 1**). For NAS glasses, the peralkaline one (NAV66.10) is yellowish, whereas the peraluminous one (NAV66.18) is brownish, indicating a different initial V speciation. To go further in the determination of V valences these colors will be quantified by optical absorption in section Optical Properties.

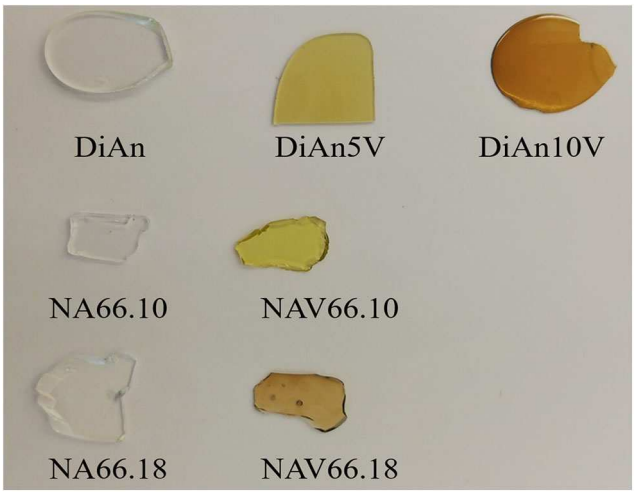

FIGURE 1 | Glasses synthesized in this study. Pristine NA66.10, NA66.18, and DiAn glasses are shown along with the V-doped ones: NAV66.10, NAV66.18, DiAn5V, and DiAn10V.

Glass Physical Properties

The physical and thermal properties of pristine and V-doped glasses are reported in **Tables 1**, **2**. Glass transition temperature values (Tg) were evaluated from DSC curves as well as the onset of crystallization (Tx) and melting temperature (Tm) for the DiAn series. The Tg does not respect the polymerization/optical basicity trend, because even if DiAn glasses are more depolymerized, they have a higher Tg than NA66.10. Indeed, Ca and Mg that are nominally considered network modifiers, have a valence of 2+, which allows them cross-linking species in the glass structure [charge compensator role; e.g., (Cicconi et al., 2016)].

The addition of vanadium induces a strong decrease of Tg for all compositions (see **Table 1**). Even if V acts as a network former, the melting point of V_2O_5 at 690°C is much lower than those of SiO_2 or Al_2O_3. It is then logical that its introduction induces a decrease of Tg. 5 wt.% of V_2O_5 causes only a moderate Tg decrease in the two depolymerized glasses, respectively, of 14°C for DiAn and 9°C for NA66.10, whereas it induces a very significant drop of 89°C in the fully polymerized NA66.18. In the different possible incorporation configurations of Vanadium in the peraluminous NA66.18 glass, one extremely likely may be its association with AlO_2^- tetrahedral units. In such a way, the VO_2^+ tetrahedral and the AlO_2^- tetrahedral will form a neutral $AlVO_4$ unit. Therefore, a part of the network modifiers is not any more charge compensating Al tetrahedral and can create additional non-bridging oxygen (NBO) lowering further the glass transition temperature.

In depolymerized glasses, Tg is driven by the collective breaking of the weakest bonds that are mostly related to the NBO and the modifier cations. In such glasses, the action of V will not

be preponderant. In the polymerized NA66.18 glass, however, V introduces weak points in the strong and very homogeneous (Si, Al) network. The behavior of V here seems to be very similar to the one of another network former, P in aluminosilicate (Mysen and Richet, 2005; Grammes et al., 2020). The DiAn series shows that the evolution of Tg is perfectly linear with increasing V content (see **Table 1**).

Two crystallizations can be detected from the DSC measurement in DiAn series. The evolution of both crystallization temperature Tx is similar to that of Tg. Therefore, the difference between Tg and Tx remains almost constant with V content. This can be understood as a measure of the glass stability (GS). The bigger the difference is between Tx and Tg, bigger is the temperature window in which the glass can be modified without crystallizing. Here the observed constant GS is contradicted by the experimental heat treatment realized since DiAn10V after 3 days at 760°C or 7 days at 735°C, shown crystallization of V_2O_5 on the surface of the samples. No crystallization was observed for the two Na-bearing glasses, as they were thermal treated (TT) 32°C above their Tg for up to 7 days. The eutectic composition DiAn has a very good glass-forming ability (GFA), which can be evaluated in terms of the Hrubÿ parameter $(Tx - Tg)(Tm - Tx)$ (Hrubý, 1972). The addition of vanadium decreases the GFA from ∼1 (DiAn) to 0.74 (DiAn5V). Remarkably, DiAn10V has a higher GFA (0.79) than DiAn5V despite the crystallizations observed. This shows the limitation of using such a parameter (Nascimento et al., 2005). Overall, V has a relatively neutral effect on both GS and GFA.

Density measurements on pristine and thermal treated glasses are reported in **Table 2**. In all cases, introducing around 1.8 mol% of V_2O_5 increases the density slightly, as expected, since V is a heavier element. The molar volume (Vm) of the glasses was deduced from the density measurement and the chemical composition (see Section Analytical Methods). The Vm increased almost linearly for all compositions and can be taken into account by using a near-constant molar partial volume of 63 ± 6 cm^3/mol for V_2O_5. This increase of molar volume is in agreement with the coordination of 4 expected for V and its network former role that opens the atomic structure of the glass. Upon TT, the density of the glasses is not changed. This proves that the effect of the cooling rate on the global glass structures is moderate and not detectable in our case. In the case of the V bearing glasses, no significant variation of the density can be seen. The results of the DiAn series are shown in detail in **Figure 2**. The dispersion of the points and the size of the error bars make it difficult to deduce any clear trend. Therefore, if during the thermal treatment some redox modifications of V took place, its effect on the volume could not be noticed.

Refractive index (n_D) increases with higher V amounts. For the DiAn series, there is almost a linear relationship ($R^2 = 0.98$) between V content and refractive index. This increase can be explained by the higher polarizability of V and/or its action as a network former in which more covalent bonds are involved and/or the possible presence of a double bond V = O. Thermal treatments induce only small variations of the refractive index (see **Table 2**).

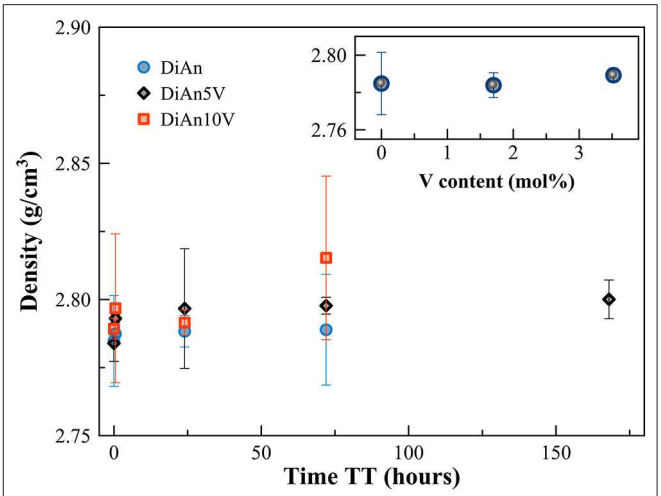

FIGURE 2 | Evolution of density with thermal treatment (TT) time for the pristine and V-doped DiAn glasses. In the inset, the density is reported against the V content (mol%).

Optical Properties

Optical Absorption

The optical absorption spectra of the samples show variations depending on vanadium concentration and thermal treatment in the range 250–1,400 nm (40,000–7124 cm^{-1}) (**Figures 3**, **4**, respectively, for DiAn and NAS glasses). Pristine glasses are colorless and show UV-edges below 300 nm, whereas the colored V-doped samples have UV-edges in the visible range around 400 nm, stopping violet light and giving the characteristic yellowish color (DiAn 5V and NAV66.10). Further shoulders of the UV-edge at 500 nm cutting blue contributions lead to the more brownish colors (DiAn10V and NAV66.18). As can also be seen between DiAn5V and DiAn10V, the total amount of V has a strong effect on the color (**Figure 1**).

The addition of vanadium shifts the UV-edge toward lower frequencies, and this redshift could be partially due to the energy gap between the valence band and conduction band which decreases linearly for higher V_2O_5 amounts (**Figure 3A**). By using a Tauc plot $(\alpha h\upsilon)^{1/2}$ against the photon energy ($h\upsilon$), the UV-edge was estimated in the same manner as for a direct optical band gap energy (**Table 3**). The UV-edge is also partially assigned to charge transfer (CT) bands of V^{5+} (Leister et al., 1999). After TT, all the glasses show a significant evolution of their absorption spectra except for DiAn5V, which stays almost constant (**Figures 3B**, **4B**). The UV-edge decreases for both DiAn samples and stays almost constant for NAV66.10 and NAV66.18. The optical absorptions increase over the full range 500–1,400 nm (2.8–1.0 eV) (as reported in **Table 3**).

Vanadium, having multiple stable valences and different local environments, can induce several bands in the UV-Vis-NIR regions. V^{5+} has a $3d^0$ electronic configuration; thus, only CT bands occur, in or around the UV region. Since CTs have very high extinction coefficients, they are not discernible from the global UV-edge. V^{4+} species ($3d^1$ electronic configuration),

TABLE 3 | Results of the optical absorption and photoluminescence studies.

	$V^{5+}/(V^{4+}+V^{5+})$ From Λ	$\%V^{3+}$	$\%V^{4+}$	$\%V^{5+}$	V^{5+} x 10^3 mol/cm^3	UV-edge (eV)	Em intensity (CPS)
DiAn5V	0.93	0.18	1.42	98.40	1.19	2.86	35,187
DiAn5V TT0.5h		0.34	1.07	98.60	1.20		33,417
DiAn5V TT1d		0.08	1.26	98.66	1.20		32,214
DiAn5V TT3d		0.09	1.26	98.65	1.20	2.60	33,121
DiAn10V	0.93	0.18	2.20	97.62	2.97	2.38	16,744
DiAn10VTT3d		0.50	0.72	98.78	3.03	1.77	16,198
NAV66.10	0.91	2.54	4.60	92.86	1.21	2.74	125,862
NAV66.10TT7d		3.98	7.36	88.66	1.16	2.84	124,877
NAV66.18	0.87	4.82	18.80	76.38	0.98	3.44	43,842
NAV66.18TT7d		7.61	22.44	69.95	0.90	3.44	46,426

Estimated percentage of each single redox species is reported, along with the concentration per volume unit of the oxidized species V^{5+} (mol/cm^3). The results below assumed that the local environment of V did not change significantly with glass composition and that the extinction coefficient of Leister et al. (1999) can be kept constant. UV-edge energies (eV) and intensities of the photoluminescence emission (Em) maxima (counts per second; CPS) are reported as well. In the first column is given the ratio between V^{5+} and V^{4+} calculated from the optical basicity Λ according to Equation [3].

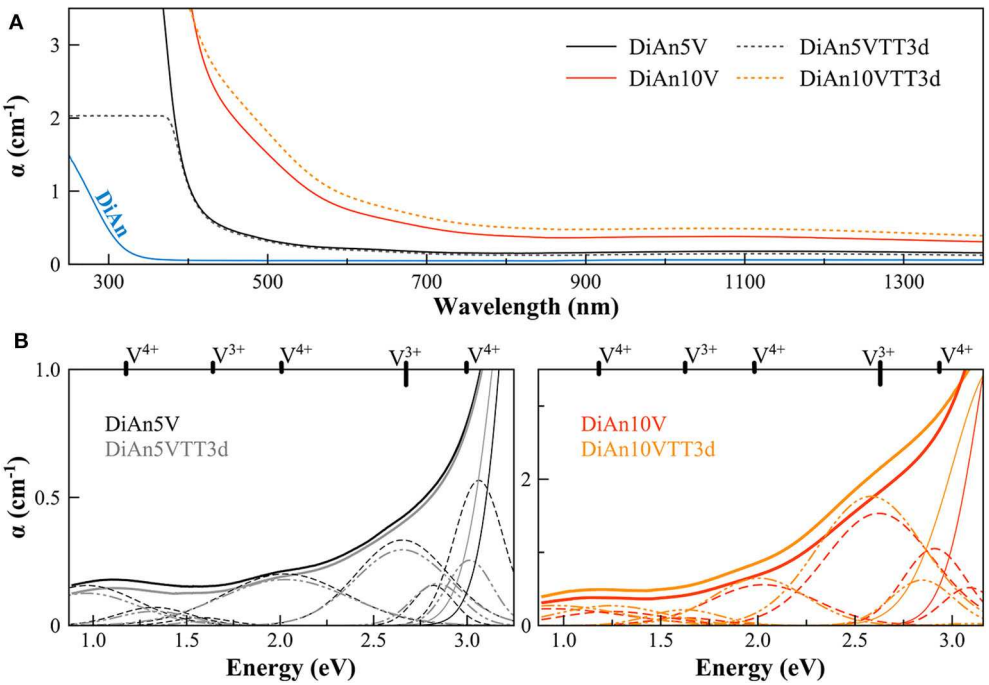

FIGURE 3 | (A) Optical Absorption spectra of pristine and V-doped DiAn glasses, melted in air, or thermally treated (TT). **(B)** Deconvolution of the optical absorption bands for V-doped DiAn glasses and 3-day thermally treated ones (TT3d).

four-fold and six-fold coordinated, should have only one spin-allowed absorption transition. However, in silicate glasses, it has been reported the occurrence of vanadyl VO^{2+} units (V = O p-bond) that yield several *d–d* transitions (Johnston, 1965a; Leister et al., 1999). In **Figures 3**, **4**, *d–d* transitions of V^{4+} (VO^{2+}) occur at ∼ 1,050 nm (∼1.2 eV; $^2T_1 \rightarrow {}^2T_2$), ∼610 nm (∼2.0 eV; $^2T_1 \rightarrow {}^2E$), and ∼420 nm (∼3.0 eV; $^2T_1 \rightarrow {}^2A_1$), and they represent the main bands in the spectra for V-doped glasses. Six-fold coordinated V^{3+} species ($3d^2$ electronic configuration) have bands at ∼700 nm (∼1.8 eV; $^3T_{1g} \rightarrow {}^3T_{2g}$) and ∼460 nm [∼2.7 eV; $^3T_{1g} \rightarrow {}^3T_{1g}$ (P)] (Johnston, 1965a; Leister et al., 1999) and references therein. These assignments are reported on the top of the **Figures 3B**, **4B**.

To go further in the determination of the proportions of the different valence species of V, these different optical absorption bands have been deconvoluted with Gaussian (G) functions (dotted and dashed lines in **Figures 3B**, **4B**). Considering the literature on band assignment and the signal deconvolution, the concentrations of V^{4+} and V^{3+} species have been estimated by considering the intensity of the bands and the molar extinction

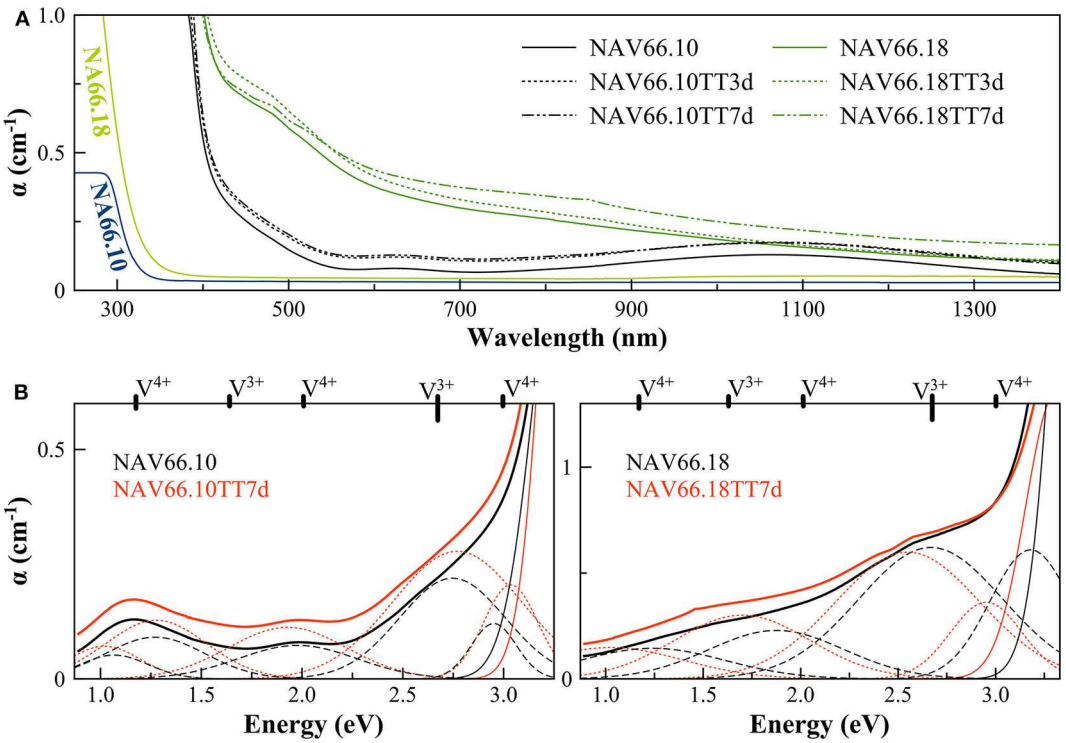

FIGURE 4 | (A) Optical Absorption spectra of pristine and V-doped NAS glasses, melted in air, and thermal treated for 3 (TT3d) and 7 (TT7d) days. **(B)** Deconvolution of the optical absorption bands for V-doped NAS glasses and 7-day thermally treated ones (TT7d).

coefficients reported by Leister et al. (1999). Here, the data treatment was difficult due to the high overlap between the different components and a strong variation of the UV-edge probably due to modification of the V^{5+} local environment and the sensitivity of the CT process to the overall redox conditions. Therefore, only two bands were used to calculate the concentration of the different V species reported in **Table 3**: the band at ∼1.9 eV for V^{4+} and the band at ∼1.6 eV for V^{3+}. The concentration of V^{5+} was deduced from the two previous data considering the total chemically analyzed content of V in the glass from **Table 1**. The proportion of V^{5+} is decreasing in the order of DiAn, NAV66.10, and NA66.18, following the same trend than the one predicted from the optical basicity, see 3.1, reported also in **Table 3**. The best agreement between the optical basicity estimation and those derived from the optical absorption spectra is for the sample NAV66.10, which is very close to the composition used by Leister et al. (1999) to determine the extinction coefficient used, i.e., 66 mol% SiO_2 and 33 mol% Na_2O. It is important to notice that to construct **Table 3**, strong approximations were done. Indeed, it was assumed that the extinction coefficients of all species can be kept constant, i.e., that the local environment of V (oxygen coordination and second neighbors) did not change significantly with glass composition. Knowing the sensitivity of transition metals to the crystal field, it is then not surprising that the results for DiAn and NAV66.18 show more discrepancies.

As can be seen from the data reported in **Table 3**, the thermal treatments change the oxidation states of the different glasses in very different ways. While for DiAn5V, no significant variations are observed, DiAn10VTT3d shows oxidation compared to DiAn10V. On the contrary, for both NAV samples, thermal treatments induced a significant reduction by a decrease of V^{5+} and a strong increase of both V^{4+} and V^{3+} contents. Theoretically, at high temperatures, reduced forms are favored and conversely, low temperatures favor the oxidized ones. Since the glasses were first melted at high temperatures and then thermally treated a little above Tg, in all cases, oxidation of V should be observed. The results here observed, with a reduction in the NAV samples, are very surprising, and no single simple explanation was found at the moment. Another unexpected result is that during the thermal treatment the ratio V^{4+}/V^{3+} stays almost constant within our uncertainties with a ratio of 3. In this paragraph, the optical absorption was only related to V^{4+} and V^{3+}. It is only on the position of the UV edge that variation related to V^{5+} content can be expected. The UV edge here stays almost constant for NAV samples. One can argue that actually, it is not a real redox modification that takes place, but rather changes of the V atomic environment, inducing a variation of the extinction coefficient. The structural evolution around V observed in this study, after several days of thermal treatment, cannot be associated with the typical structural relaxation of glass, which takes only some couple of minutes at Tg. To confirm the observation done by optical

spectroscopy, the study of the photoluminescence can provide complementary information.

Photoluminescence

Photoluminescence (PL) spectra of V-bearing DiAn and NAS glasses are reported in **Figure 5**, and the maximum emission intensities for the different glasses are provided in **Table 3**. The pristine glasses had very weak luminescence due to iron impurities, with intensity by two orders of magnitude lower compared to the V-bearing one and so were omitted here. The excitation spectra were recorded using the intensity of the luminescence at the maximum of the emission spectra (see arrows in **Figures 5B,C**). All spectra shown in **Figures 5B,C** have been normalized to the total area to better discern the differences.

The PL spectra of V glasses show a very broad emission (Em) band centered between 580 and 591 nm, depending on the glass composition. By increasing V content, between DiAn5V and DiAn10V, the maximum of the emission redshifts by 7 nm, and its intensity strongly drops (>50% intensity drop). For alkali-bearing glasses, by going from NAV66.10 to NAV66.18, the maximum of the emission redshifts by 5 nm and its intensity decreases almost by factor 3 (**Figure 5A**). In the latter two glass systems, the amount of vanadium is almost constant; thus, the variations have to be related to the bulk chemistry. The position of the emission maximum and its overall shape does not change significantly during thermal treatment for any sample, whereas the intensity of the emission lines presents small variations depending on the thermal history. Hence, on one hand, bulk chemistry and total V content do not strongly influence the broad emission band position, while on the other hand, the photoluminescence emission intensity shows very strong differences, depending on vanadium content or glass composition.

The broad excitation (Ex) band, split into two discernible contributions: a smaller one at 280 nm, which is the more pronounced in the NAV66.10 series, and the strongest one between ~335 and 350 nm, which presents a shoulder at

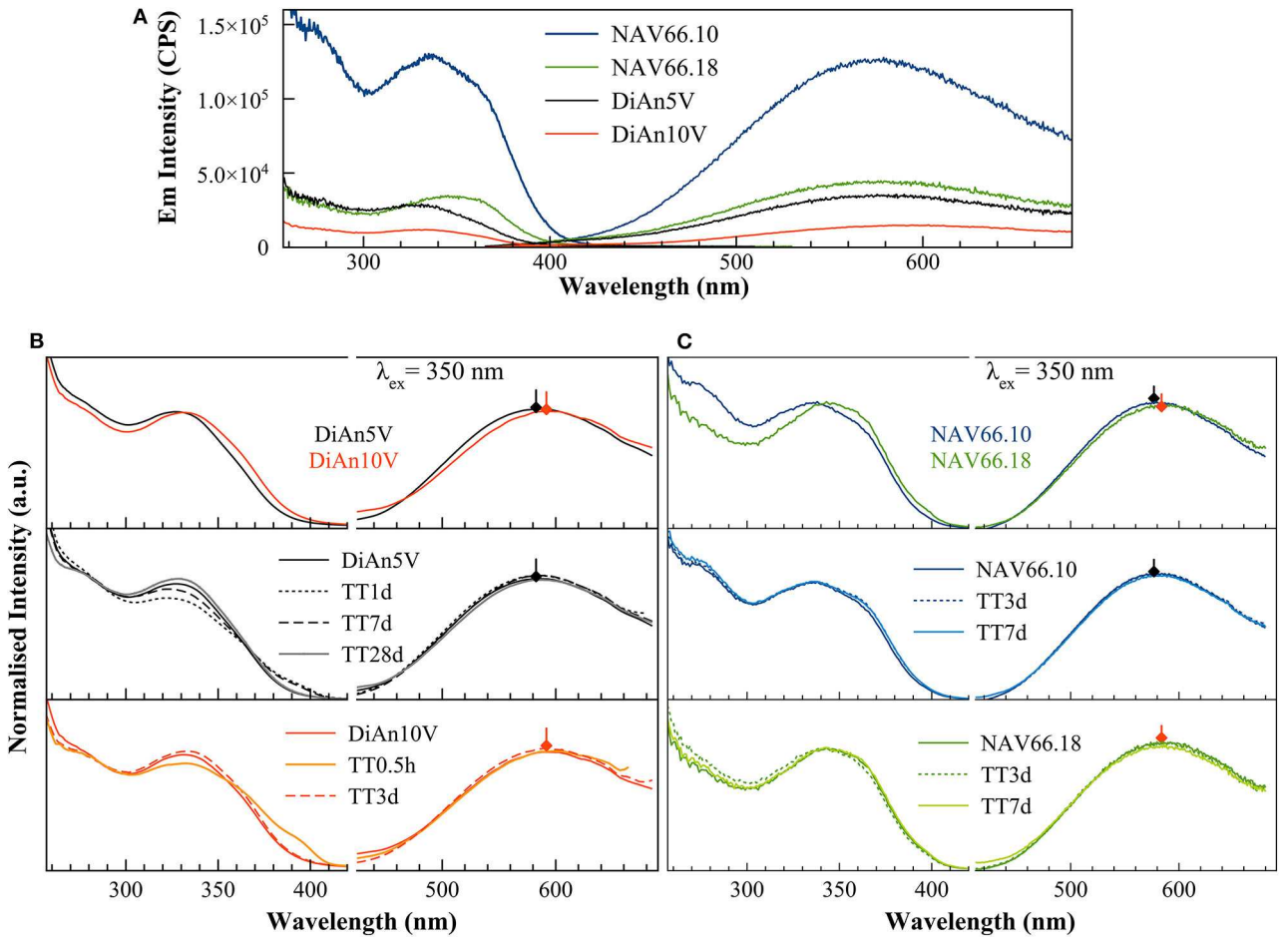

FIGURE 5 | (A) Raw excitation and emission spectra of V-doped DiAn and NAS glasses. There is an intensity drop of the photoluminescence emission depending on the bulk composition. **(B)** Excitation (Ex) and Emission (Em) spectra of V-doped Dian glasses normalized to their total area. The increase of V content induces a redshift of both Ex and Em. TT above 3 days as well-produced changes in the excitation lines. **(C)** Normalized photoluminescence spectra for NAS glasses. The increase of the Al/Na molar content induces a redshift of both Ex and Em bands.

∼360 nm (**Figure 5**). The position of the stronger band redshifts and the relative intensity of the shoulder at 360 nm increases in the order DiAn5V, DiAn10V, NAV66.10, and NAV66.18, following therefore the optical basicity trend. While this stronger band position moves, the peak at 280 nm and the shoulder at ∼360 nm do not change. Thermally treated glasses (**Figures 5B,C**) show variations that are not linear with TT time and differ for each composition. Nevertheless, TT glasses present small differences in the emission intensity and also in the relative intensity of the excitation shoulder at 360 nm. Similar complex behaviors were also observed in the optical absorption spectra in section Optical Absorption.

The excitation spectra can be attributed to CT processes related to V^{5+} groups. These processes involve an electron transfer from the double-bonded O^{2-} to V^{5+} inducing the formation of transitory V^{4+} species from which radiative decay is responsible for the emission (Anpo et al., 1980; Kniec and Marciniak, 2019). Previous studies done on crystalline materials highlighted that the frequency of the oxygen–vanadium charge-transfer excitation band provides information regarding the number of oxygen ligands surrounding vanadium. Indeed, by increasing oxygen coordination around V^{5+} species from 4 to 6, the absorption bands redshift from ∼275 and ∼340 to ∼400 to ∼470 cm^{-1}, as observed for $NaVO_3$ ($^{[4]}V^{5+}$), VPO_4 ($^{[5]}V^{5+}$) and V_2O_5 ($^{[6]}V^{5+}$), respectively (Schraml-Marth et al., 1991; Kornatowski et al., 1995) and references therein.

In our glasses, because of the presence of a split excitation, and because their frequency positions resemble the ones reported for $NaVO_3$ (Schraml-Marth et al., 1991), we assigned the small band at around 280 nm and the main band in the range of 330–360 nm to $\pi(t_{1,2})$ to d(e) oxygen-to-$^{[4]}V^{5+}$ CT transitions with oxygen in apical position (V = O) (Schraml-Marth et al., 1991; Dzwigaj et al., 2000). Other CT transitions at higher wavelengths, as in the case of oxygen-to-octahedral V^{5+} transition, are not present in any of the glasses investigated here. Thus, we can assume that at least two different kinds of $^{[4]}V^{5+}$ species are present in the glasses, that differ according to the distortion of the site, and in turn, according to the first neighbor ligands.

To go further in the link between this CT and the photoluminescence, it could be checked if the emission intensity is correlated to the quantity of V^{5+} previously determined using optical absorption and the extinction coefficient of Leister et al. (1999) (see section Analytical Methods). Since in the photoluminescence spectrometer the excitation is realized in the volume of the sample, it is more appropriate to use the volume concentration of V^{5+} in mol/cm^3, which can be obtained using the density. Such correlation is reported in **Figure 6A**. An overall trend highlights that higher amounts of oxidized species induce lower emission intensity and thus, a quench of the photoluminescence. The reason for this quenching is principally related to self-absorption. However, in the concentration region, the emission intensity of NAV66.10 (represented in light blue in **Figure 6A**) is much higher, suggesting that V^{5+} species contained in this glass have a special configuration enhancing CT processes.

The excitations identified here at 280 and 350 nm correspond to the energy of the UV-edge observed in the optical absorption study. The link between the two observations is confirmed by the very good correlation between the emission intensity and the UV-edge, as shown in **Figure 6B**. The lower energy position of the UV-edge can be correlated with the number of non-bridging oxygen, and to the bond strength (e.g., Hensler and Lell, 1969; Laorodphan et al., 2016), thus the trend observed agrees with depolymerization, and in turn, with the thermal and physical property variations observed for these glasses. However, here again, the sample NAV66.10 that had an exceptionally high photoluminescence emission and an intermediate polymerization falls above the observed correlation. To explain such high emission intensity compared to the other glass compositions, we could take into account the low absorption coefficient in the visible region of the peralkaline NAV66.10 sample, and thus, the possibility of having self-absorption of the fluorescence in all other compositions. All the same, there is not a linear correlation between the absorbance values at 580 nm and PL emission intensity, and the shape of the photoluminescence emission spectra is almost identical for all glasses. Thus, NAV66.18 emission is only marginally lowered by self-absorption. PL emission intensity variations should be explained by other mechanisms, most probably related to V local surrounding. Only further structural observation can help to identify the local structure of V^{5+} responsible for such a high CT capacity.

Glass Structure

In **Figure 7** are reported the parallel (VV) and cross-polarized (VH) Raman spectra of pristine and V-bearing DiAn and NAS glasses. Raman spectra of V-bearing glasses show vibrational modes both related to vanadium and silicon groups that mainly overlap in the frequency range of about 700 to 1,000 cm^{-1}.

The Raman spectrum of the pristine DiAn glass has distinct contributions, typical of a Ca-Mg aluminosilicate glass containing ∼50 mol% SiO_2 (Mysen et al., 1979; Mysen and Richet, 2005). Raman vibrations related to the pristine NAS glasses are discussed in details in (Cicconi et al., 2017). In the pristine aluminosilicate glasses, the main vibrations occurring in the frequency region between 400 and 800 cm^{-1} were assigned to T-O-T intertetrahedral linkages and breathing vibrations of 4- and 3-ring members (defect bands D_1 and D_2; where T represents the tetrahedrally coordinated cation, i.e., Al a/o Si). The main band position decreases as expected with polymerization: 580 cm^{-1} for DiAn, 510 cm^{-1} for NAV66.10, and 490 cm^{-1} for NAV66.18. In the high-frequency region (850–1,300 cm^{-1}) there is the so-called *Q*-range, where vibrations related to Si-O asymmetric stretching can be found. This region shifts to higher frequency with polymerization. Si-O-Si ring and Si-O stretching motions are strongly polarized bands, thus, their intensity drastically decreases when collected as cross-polarized (VH). Indeed, the polarization ratio (PR), that is the intensity ratio between the perpendicular and the parallel components of Raman scattered light $PR = \frac{I_{VV}}{I_{VH}}$ is > 2.5, indicating highly polarized bands.

The Raman spectra of doped DiAn5V and DiAn10V glasses, compared to the pristine one, show additional intense vibration modes, indicating the combined presence of modes both related to the silicate network and to the vanadium ones (marked in

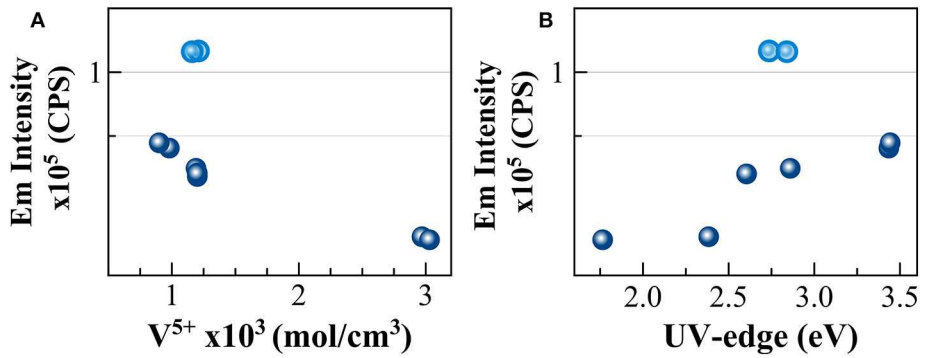

FIGURE 6 | Correlation between the intensity of the photoluminescence emission and **(A)** concentration for volume unit of V^{5+} species and **(B)** UV-edge energy (eV). Light blue circles identify NAV66.10 glasses.

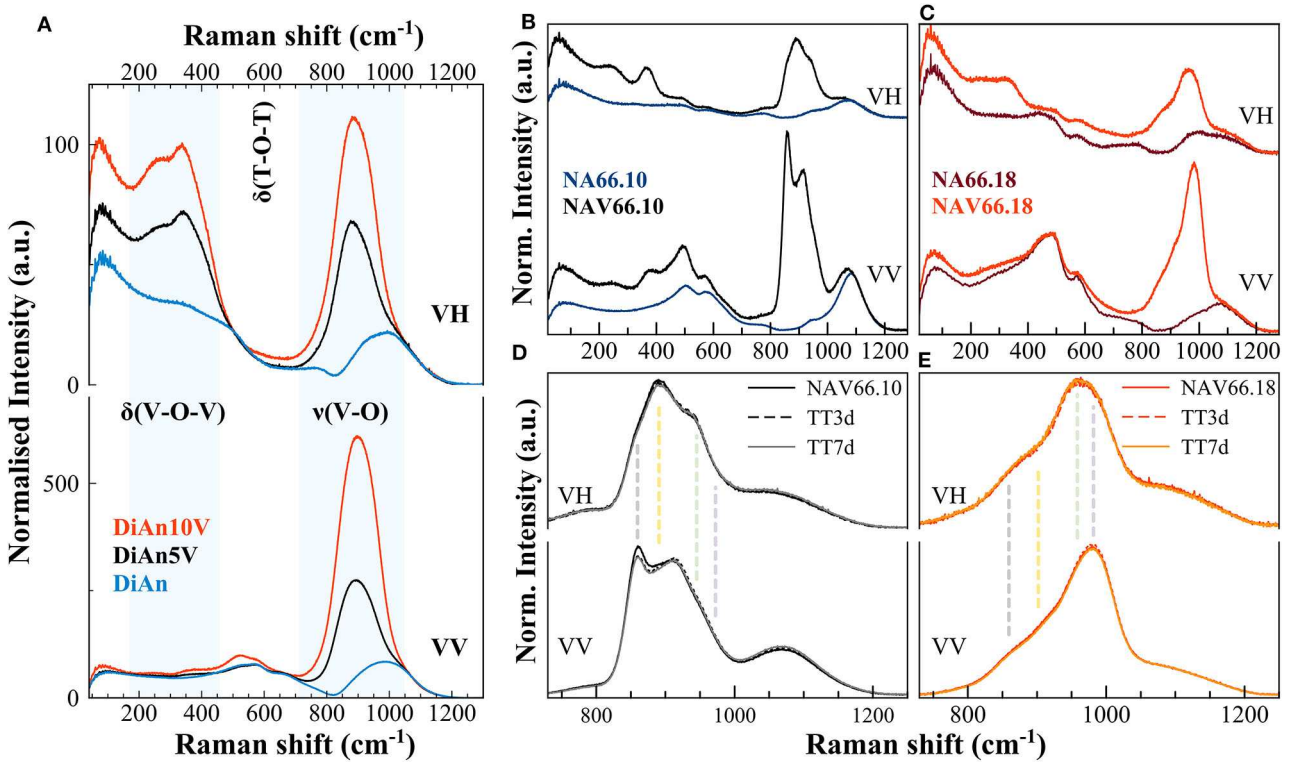

FIGURE 7 | (A–C) Parallel (VV) and cross-polarized (VH) Raman spectra of pristine and V-bearing DiAn and NAS glasses, respectively. Shaded areas highlight the vibrations related to the V networks. Si-O-Si ring and Si-O stretching motions are highly polarized bands; thus, their intensity drastically decreases when collected as cross-polarized. **(D,E)** Raman spectra of V-bearing NAS glasses after thermal treatments above Tg, of 3 (TT3d) and 7 days (TT7d). Vertical dashed lines highlight the different vibrations, each related to distinct V species (see text for details).

Figure 7A). In the low-frequency region (~150–500 cm^{-1}) there are depolarized bands related to bending vibrations of trigonal VO_5 bipyramids (Attos et al., 1997). In the high-frequency portion, above 700 cm^{-1}, a strong asymmetric band rises when vanadium is added, and its intensity increases by increasing V content. This broad band might contain several vibrations, both related to symmetric stretching of V-O-V bonds in penta-coordinated VO_4 groups (tetragonal pyramid $V^{4+}O_5$ at ~885 cm^{-1}), and at least three stretching modes of $V^{5+}O_4$ tetrahedra with a V =O apex between 900 and 1050 cm^{-1} (Attos et al., 1997 and references therein). The broad band partially overlaps with the silica asymmetric stretching modes, making vibrations assignment very difficult, with the presence of V masking most of the contributions of the aluminosilicate network. Precise observation of the silica Main band and of the D_2 band between 500 and 700 cm^{-1}, as well as the region of the Si-O stretching

modes above 1,100 cm^{-1}, present no significant modification. The introduction of up to 4.8 mol% of V_2O_5 does not perturb significantly the aluminosilicate network.

The Raman spectra of alkali-bearing glasses strongly differ as well when containing vanadium (**Figures 7B,C**). However, as for DiAn, in the regions not affected by the vibrations related to V species, the aluminosilicate network remains almost unchanged. In V-doped peralkaline glass (NAV66.10) several prominent features are related to the V network (vertical dashed lines in **Figures 7D,E**). In the low-frequency region, the bending vibrations of trigonal VO_5 bipyramids (∼250 and ∼370 cm^{-1}) are strong, and these bands are highly depolarized (**Figure 7B**). In the high-frequency region, vanadium vibrations are rather well-separated from the silica stretching modes. In the peralkaline glass, the complex nature of the strong vanadium band centered at ∼900 cm^{-1} is undoubtedly discernible, with the split of the main peak in two components. Additionally, another side contribution is clearly visible at 960 cm^{-1}. Moreover, the cross-polarized spectrum of NAV66.10 glass highlights the presence of a depolarized band, centered at ∼893 cm^{-1} (vertical dashed lines in **Figure 7D**). In the peraluminous glass (NAV66.18), the vanadium vibrations in the high frequency (HF) portion are shifted at higher values (maximum at ∼ 980 cm^{-1}) (**Figures 7C,E**). Moreover, the whole band is particularly asymmetric, with the barycenter moved ∼70 cm^{-1} toward higher frequencies. In the low-frequency region, the bending vibrations of trigonal VO_5 bipyramids were shifted at lower frequencies and were broader and weaker compared to the peralkaline glasses, suggesting a different distribution of the vanadium species (**Figure 7C**). Based on studies done on SiO_2 and silicate glasses, the positive anti-symmetrical variation between vanadium low- and high-frequency envelopes, together with the shift toward higher wavenumber of the HF portion, might indicate shorter V–O bond length and higher degrees of polymerization.

Since the majority of vanadium ions are oxidized (V^{5+} > 90%; see **Tables 1**, **3**) the complexity of the vibrations might be explained by the occurrence of several V^{5+} species, with configurations resembling the ones of P^{5+} species. Hence, some assumptions on the possible V–O bonding and first neighbors can be done, commensurate with the glass chemistry and the correspondences with the P^{5+} species. Likely, all Al, Si, and V atoms are exclusively tetrahedrally coordinated, and four-fold coordinated vanadium atoms, depending on the kind of neighbors can have several configurations. For instance, the excessing amount of Na^+ ions in the peralkaline glass could lead to the formation of metavanadate units in which a V^{5+} tetrahedral is connected only by one oxygen to the network. Whereas, the availability of Al ions in the peraluminous glass favors the creation of neutral $AlVO_4$ units by the association of vanadium VO_2^+ tetrahedral units with AlO_2^- ones. Other possible species involve V atoms that are tetrahedrally coordinated to two or three bridging oxygen (BO). This complexity could be represented by using the Q^n-species notation, similarly to the one used to represent Si^{4+} and P^{5+} connectivity. Indeed, Q represents a four-fold coordinated cation, and the apex n denotes the number of BO. In a tetrahedral, the more you have BO, the higher the covalency of the bond is between the central cation and the oxygens. Therefore, the Q^n species vibrate at a higher frequency when n increases.

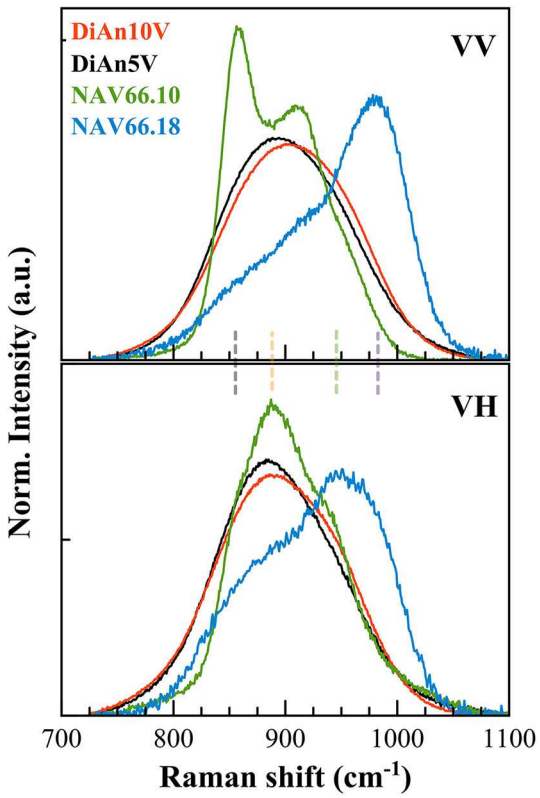

FIGURE 8 | Polarized V signals have been extracted by a direct subtraction of the respective pristine glass signals and normalized on the total area. The extracted spectra highlight the vibrations exclusively coming from V. Four main contributions can be discriminated at ∼855, 890, 960, and 985 cm^{-1} (vertical dashed lines, as in **Figures 7D,E**).

As can be seen in **Figure 7**, the doped glasses are always appearing in excess compared to the respective pristine glasses, because of the strong vanadium vibration modes. It is then possible to extract the signal exclusively coming from the V vibrations by making a direct subtraction of both spectra. The exclusive Vanadium Raman contributions are plotted in **Figure 8** for all glasses (the polarized signals are renormalized to the total area). Here, clearly, the four different contributions can be appreciated in all glasses, albeit with different intensities depending on glass chemistry or vanadium content. In detail, four contributions can be discriminated which are much more evident in the alkali aluminosilicate glasses: at ∼855, ∼890; ∼960, and ∼985 cm^{-1} (vertical dashed lines, as in **Figures 7D,E**). For the DiAn series, only a large envelop embedding the different V species could be observed until now. All the same, despite the broad band, in the subtracted spectra in **Figure 8**, we can observe a shift toward higher frequencies for DiAn10V, from which three considerations can be done: (i) a higher vanadium content induces the increase of the vibration at higher frequencies (∼985 cm^{-1}), at the expenses of the one at ∼890 cm^{-1}; (ii) the position of the dashed lines deduced from the NAS glasses perfectly

reproduce the shoulders observed in DiAn glasses above 850 cm^{-1}; and (iii) a further vibration is present in DiAn5 and DiAn10V glasses, at a lower frequency of ∼815 cm^{-1}.

In order to discriminate the different possible vanadium populations, we used the polarizability of the vibration modes calculated as ratio PR between the parallel and the cross-polarized components after the subtraction and before renormalization. This approach allowed us to evaluate graphically the polarizability (that means the symmetric or asymmetric nature of the vibration) of the different components that are embedded in the broad frequency region between 700 and 1,300 cm^{-1}. **Figure 9** reports the calculated PR of the different V-doped glasses and the probable V^{5+} species associated with each contribution. Indeed, based on the considerations done above and on the extent of the degree of polarizability, four probable Q^n species have been taken into account. By looking at the Raman spectra reported in **Figure 8** and to the PR in **Figure 9**, it is clear that the main peak at ∼850 cm^{-1} in NAV66.10 glass is highly polarized with its PR = 3.4. Likewise, the other intense band centered at 917 cm^{-1} is nearly doubled in parallel polarized spectra. Thus, these two contributions must represent asymmetric V^{5+} species, such as the ones related to Q^1 and Q^3 species. Since the only glass having such sharp prominent features was the peralkaline one, it is rational to assign the band at ∼850 cm^{-1} to Q^1 species connected to Na ions, and the band at ∼917 cm^{-1} to V = O apex of the V^{5+} species. Conversely, in the peraluminous glass, the most prominent feature was at ∼985 cm^{-1}. This vibration is likely related to the association of vanadium with AlO_2^- tetrahedral units. To support this notion, there are two pieces of evidence: (i) this band has a higher frequency position and (ii) the lower polarizability, compared to the V = O apex band. Moreover, NAV66.18 is the only glass with an exceeding amount of aluminum ions compared to network modifiers ones. The V–Al relationship, associated with the creation of NBO in the network could explain the extremely high drop of Tg seen for the peraluminous glass.

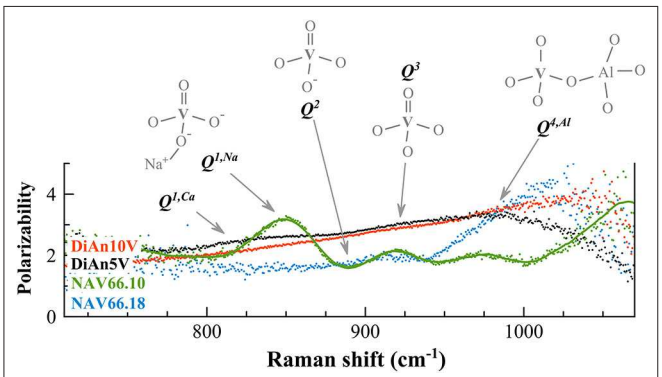

FIGURE 9 | The calculated polarization ratios of the different V-doped glasses (polarizability) allowed us to discriminate the different vibrations in the Raman frequency range between 750 and 1,050 cm^{-1} exclusively related to vanadium. To each contribution is associated the probable V^{5+} species responsible for the vibration. Details of the V species are reported in the text.

V-doped DiAn glasses have a broader band that englobe all possible V-vibration modes, and an almost constant PR = 2.5, from which almost no contributions at 850 and 917 cm^{-1} are distinguishable in **Figure 9**. Only a broad weak band is visible (∼815 cm^{-1}), that might be associated to metavanadate units in which a V^{5+} tetrahedral is connected only by one oxygen to the aluminosilicate network, and has Ca^{2+} ions connected to the NBO ($Q^{1,Ca}$). This uniform behavior can be explained by the lesser localization of the alkali earth cation modifier, compared to Na. Furthermore, it is known on phosphate glasses that the electron of the double bond is not localized giving an identical charge to the apical O and the NBOs (Brow et al., 1995). If that is also the case for V, it is then understandable that the distinction between Q^1, Q^2, and Q^3 species is difficult to make and that a large continuum exists.

This new understanding of the V structure can help us to attempt a better assignment of the atomic environment underlying the V^{5+} CTs noticed in section Photoluminescence. It was observed that this CT was very intense in NAV66.10 and decreased by a factor 2 in NAV66.18 and DiAn5V. The preponderant presence of $Q^{4,Al}$ structure in NAV66.18 is associated with a disappearance of the apical oxygen which prevents the formation of the V^{4+} excited state needed for the CT. Overall NAV66.10 and DiAn5V present both low *n* Q species significantly polarizable. The main structural difference between them is the sharp Q^1 population present only in NAV66.10, which presents simultaneously an apical oxygen, and well-localized NBO. It is reasonable to assert that the CT luminescence observed is associated with these $Q^{1,Na}$ units.

Thermal treated glasses (3 days; label TT33d) show almost no variations in the Raman vibrational bands related to the distribution of apical oxygens and VO_4 units of DiAn glasses. Only the DiAn5V high frequency envelop has a slightly lower VO_4 component, and changes are limited to relative intensities and not on band positions. Thermal treatments of NAV66.10 composition induces small visible structural changes. Deconvolution of the Raman signals in the frequency range 700–1250 cm^{-1} highlights the decrease of the area related to the Q^1 contribution (∼ −8%) after 7 days of thermal treatment. Thermal treatment of the peraluminous sample induces also only small changes depending on the time. After 3 days (TT3d) there is an intensity decrease of the silica D_2 defect line and an intensity increase (∼ +2%) of the band at 980 cm^{-1}. Overall, thermal treatment does not produce visible changes on the aluminosilicate network.

Mechanical Properties

The Brillouin spectra were collected in two different geometries: backscattering and platelet geometry (Kieffer, 2015). In the platelet geometry, both longitudinal and transversal acoustic modes can be observed. Typical Brillouin spectra in platelet and backscattering geometry are given in **Figure 10** for DiAn and NAS samples. The Poisson ratio, ν, can be obtained directly from the ratio between the transverse and longitudinal Brillouin shift. Theoretically, the platelet geometry is enough to get the sound velocities and from them using the determined densities to deduce all the elastic moduli. However, the data then obtained

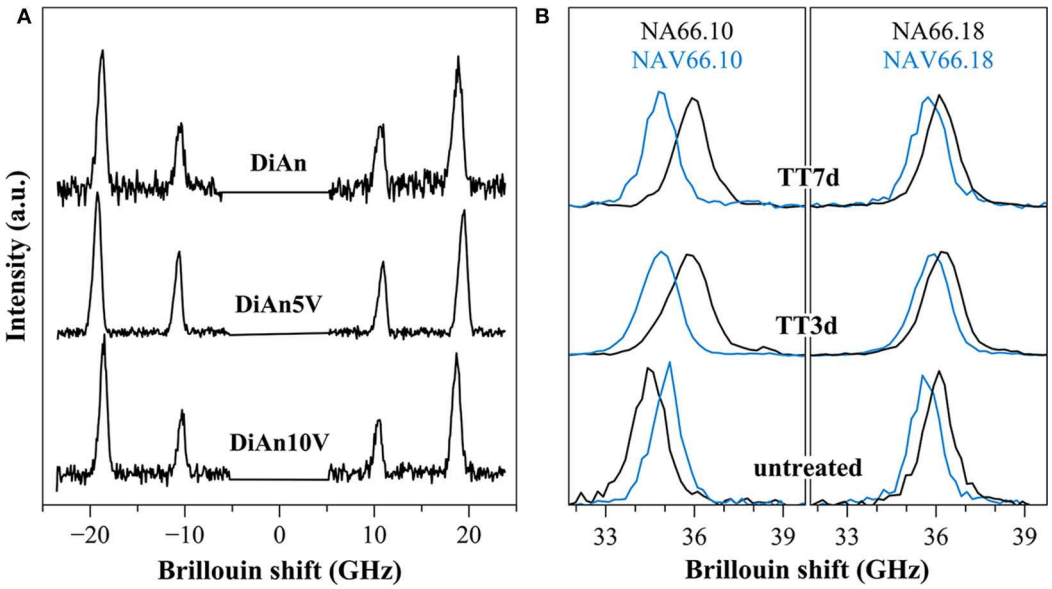

FIGURE 10 | (A) Brillouin spectra for pristine DiAn and V-bearing glasses collected in platelet geometry, where both longitudinal and transversal acoustic modes can be observed. **(B)** Example of Brillouin spectra collected in backscattering geometry for V-free and V-doped NA66.10 and NA66.18 glasses. The evolution of the signals for different thermal treatment times (3 and 7 days) is shown.

TABLE 4 | Elastic properties (GPa) and Brillouin shift (GHz) of all.

	ν	ν *Calc.*	M (GPa)	*M Calc.*	G (GPa)	K (GPa)	E (GPa)	Brillouin shift (GHz)
±	0.004		0.5		0.9	0.8	2.5	0.1
DiAn	0.273	0.261	123.4	111.4	38.5	72.1	98.0	43.7
DiAn5V	0.274	0.261	121.6	111.0	37.9	71.1	96.5	43.5
DiAn10V	0.275	0.261	112.4	110.3	34.9	65.9	88.9	42.4
NA66.10	0.224	0.240	77.0	85.1	27.4	40.5	67.0	34.5
NAV66.10	0.224	0.240	77.3	85.4	27.5	40.7	67.3	35.1
NA66.18	0.215	0.238	82.5	94.1	29.9	42.6	72.7	36.1
NAV66.18	0.214	0.238	79.8	93.6	29.0	41.1	70.5	35.7

The Brillouin shift reported here was obtained in backscattering configuration at 488 nm wavelength and allowed determining the longitudinal modulus M. The Poisson's ratio, ν, is calculated from platelet geometry not reported here. All the other elastic parameters are deduced from M and ν. Calc.: calculated according to the Makishima and Mackenzie (1973) model.

are very sensitive to the angle used, which is difficult to determine with high enough precision. To reduce the uncertainty, the backscattering geometry, where no angle problem can occur, was complementary used. The backscattered Brillouin shifts are reported in **Table 4**. Using the refractive index, corrected at 488 nm using the Abbe number, and the aforementioned backscattered Brillouin shift, the longitudinal modulus M can be determined. Then, by using both ν and M all the elastic parameters are deduced (see **Table 4**). Later in this section, only ν and M will be discussed, since they are the values closest to measurements. The values found are in agreement with previous studies on similar systems (Pönitzsch et al., 2016; Weigel et al., 2016).

Within each series, it can be noticed that ν stays constant, which means that the addition of V or the thermal treatment are not affecting ν. On the contrary, M evolves differently with the addition of V, for each series. In the DiAn series, on average, M decreases by 1.7% for each mol of V_2O_5 added. In the NA66.10, M stays constant with the addition of V. And in what could look surprising, it also decreases by 1.7% for each mol of V_2O_5 added in the NA66.18 series.

Elastic properties have a complex evolution with composition. The model developed by Makishima and Mackenzie (1973) can help us to better understand the evolutions here observed. This model takes into account two parameters: the atomic packing volume and the dissociation energy per unit volume. The packing volume increases with the network polymerization in the order of DiAn, NA66.10. and NA66.18. It increases also with the addition of V_2O_5, following the evolution of the molar volume discussed in section Glass Chemistry, V Redox

State, and Optical Basicity. At the opposite end, the dissociation energy is more sensitive to the elements and especially to the presence of Na, which strongly decreases it. Using this model and the parameters revised by Inaba et al. (2000) theoretical values of both ν and M were calculated and reported in **Table 4**. The values experimental and theoretical significantly differ. The model always overestimates the elastic moduli for the DiAn series and underestimate those for the sodium-bearing glasses. However, the model respects the trend observed, not only between the series, but also with the addition of V_2O_5. Indeed, for both series DiAn and NA66.18, the addition of V induces a decrease of M around 0.25% per V_2O_5 mol added and predict an increase in the case of NA66.10 (see **Figure 11**). The agreement on the trend is very interesting because it underlines the importance of dissociation energy. Its lack of precision shows also its limitation. A similar disagreement was already shown for aluminosilicate glasses (Eagan and Swearekgen, 1978; Inaba et al., 2000; Lin and Liu, 2006; Pönitzsch et al., 2016), and many factors were proposed to explain these disagreements. The calculations can depend a lot on the coefficient use and especially the way to determine properly the atomic packing density (Lin and Liu, 2006; Pönitzsch et al., 2016). The usefulness of the atomic packing density was recently questioned by Zeidler et al. (2014), since the oxygen radius can change a lot. Moreover, the approach of Makishima and Mackenzie only takes into account the mean volumetric values and does not consider the topology of the network. In the case of partially covalent bonds, like in the system investigated here, local intertetrahedral angles have a strong effect on the elastic properties as shown by the non-linear evolution of the Brillouin shift with pressure in sodium aluminosilicate glasses (Sonneville et al., 2013).

No significant variations of the mechanical properties were observed with thermal treatment.

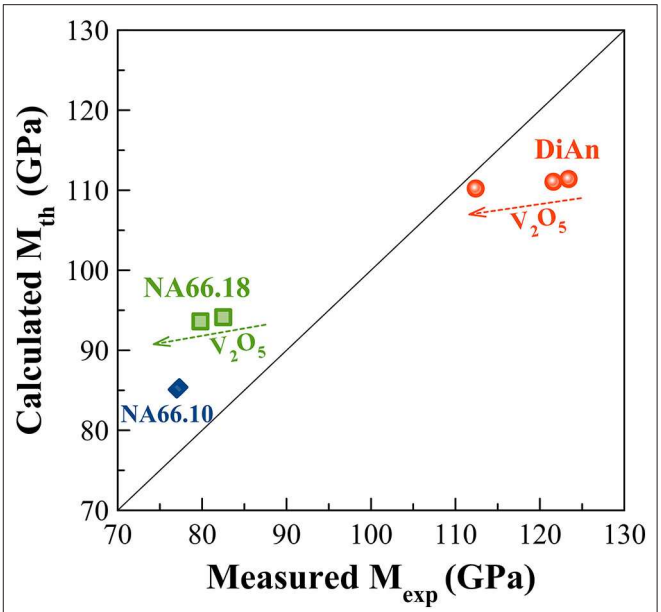

FIGURE 11 | Experimental Longitudinal modulus (M_{exp}) against the Theoretical one (M_{th}) calculated according to the Makishima and Mackenzie (1973) model. The calculated values always overestimate the elastic moduli for the DiAn series and underestimate those for the sodium aluminosilicate glasses. However, the model respects the experimental trends observed not only between the series but also with the addition of V_2O_5.

CONCLUSIONS AND FINAL REMARKS

A large screening of the properties of Vanadium-bearing aluminosilicate glasses was realized through the study of three glasses, having very different network polymerizations. This work complements the very low number of data related to this element in silicates glasses. First of all, we verified that the bulk chemistry (presence of alkali or alkaline-earth ions, Al/Na molar ratio) has a first-order influence on the vanadium speciation, and in turn, on the optical properties. These changes in speciation, evidenced by the different glass colors, were realistically quantified using optical absorption spectroscopy. However, complementary investigations using ESR or XPS spectroscopies would permit to improve the extinction coefficients' reliability.

The average redox state of vanadium and its site symmetry can be modified just above Tg. Thermal treatments induce changes in the vanadium speciation (average oxidation state, bond distances, and oxygen coordination) and on the evolution of V^{3+} V^{4+} and V^{5+} proportions. The variations observed on the vanadium redox state upon thermal treatment are still too narrow in the investigated conditions to produce clear variations on the glass network and the mechanical properties.

Because of the versatility of this element, straightforward structure–property relations are difficult to establish. The structural role of Vanadium needs to be better understood in a more fundamental way. The strong drop in the glass transition temperature, as well as the reduction of the mechanical properties for some compositions, could suggest a modifier role of Vanadium. However, no proof of associated depolymerization of the silicate network could be observed. The Vanadium seems to act as a network former, partially connected to the silica aluminate network. A close observation of the vibrations involving V and their polarizability using Raman spectroscopy shown that V is surrounded by one to four bridging oxygens. The chemistry of the glass has a strong effect on the repartition of these different environments. This new attempt to describe the V network would certainly benefit from complementary NMR studies, or more in general, element selective techniques.

For the photoluminescence properties, the change of chemistry did not affect the wavelength of the large yellow emission of Vanadium, making it a not-easily tunable phosphorous. At the opposite end, its intensity is enhanced dramatically with the presence of Na. The CT mechanism underlying the emission was assigned to four fold coordinated V^{5+} having an apical oxygen (V = O) and surrounded by two non-bridging oxygens.

The addition of V in the sample NA66.10 has shown simultaneously a decrease of the Tg of 20 K, constant glass

stability, and no change of the mechanical properties. This result is very encouraging in view of the efforts currently considered to reduce energy consumption. The introduction of V in the formulation of glass for which transparency is not an issue as reinforcement fibers could be a very promising solution.

DATA AVAILABILITY STATEMENT

The raw data supporting the conclusions of this article will be made available by the authors, without undue reservation.

AUTHOR CONTRIBUTIONS

DL, DB, and LW designed the project, provided funds and supervised the progress. MC, ZL, and TU performed experiments, and data analysis. MC and DL did the data interpretation and wrote the article. All authors contributed to the article and approved the submitted version.

FUNDING

This work was supported by Deutsche Forschungsgemeinschaft (DFG) project PP1594: Topological Engineering of Ultrastrong Glasses.

ACKNOWLEDGMENTS

The authors thank the people of the Glas group WW3 Erlangen for the help and the useful discussions. We would like to thank two reviewers for their constructive comments.

REFERENCES

Anpo, M., Tanahashi, I., and Kubokawa, Y. (1980). Photoluminescence and photoreduction of vanadium pentoxide supported on porous Vycor glass. *J. Phys. Chem.* 84, 3440–3443. doi: 10.1021/j100462a026

Attos, O., Massot, M., Balkanski, M., Haro-Poniatowski, E., and Asomoza, M. (1997). Structure of borovandate glasses studied by Raman spectroscopy. *J. Non Cryst. Solids* 210, 163–170. doi: 10.1016/S0022-3093(96)00596-0

Brow, R. K., Tallant, D. R., Myers, S. T., and Phifer, C. C. (1995). The short-range structure of zinc polyphosphate glass. *J. Non Cryst. Solids* 191, 45–55. doi: 10.1016/0022-3093(95)00289-8

Cicconi, M. R., De Ligny, D., Gallo, T. M., and Neuville, D. R. (2016). Ca neighbors from XANES spectroscopy: a tool to investigate structure, redox, and nucleation processes in silicate glasses, melts, and crystals. *Am. Mineral.* 101, 1232–1235. doi: 10.2138/am-2016-5663

Cicconi, M. R., Giuli, G., Ertel-Ingrisch, W., Paris, E., and Dingwell, D. B. (2015). The effect of the [Na/(Na+K)] ratio on Fe speciation in phonolitic glasses. *Am. Mineral.* 100, 1610–1619. doi: 10.2138/am-2015-5155

Cicconi, M. R., Neuville, D. R., Blanc, W., Lupi, J. F., Vermillac, M., and De Ligny, D. (2017). Cerium/aluminum correlation in aluminosilicate glasses and optical silica fiber preforms. *J. Non Cryst. Solids* 475, 85–95. doi: 10.1016/j.jnoncrysol.2017.08.035

Cody, G. D., Mysen, B., Sághi-Szabó G., and Tossell, J. A. (2001). Silicate-phosphate interactions in silicate glasses and melts: I. A multinuclear (27Al,29Si,31P) MAS NMR and ab initio chemical shielding (31P) study of phosphorous speciation in silicate glasses. *Geochim. Cosmochim. Acta* 65, 2395–2411. doi: 10.1016/S0016-7037(01)00597-X

Dietzel, A. (1948). Glasstruktur und Glaseigenschaften. *Glastechn. Ber.* 22, 41–50.

Duffy, J. A. (1993). A review of optical basicity and its applications to oxidic systems. *Geochim. Cosmochim. Acta* 57, 3961–3970. doi: 10.1016/0016-7037(93)90346-X

Duffy, J. A. (1996). Redox equilibria in glass. *J. Non Cryst. Solids* 196, 45–50. doi: 10.1016/0022-3093(95)00560-9

Dzwigaj, S., Matsuoka, M., Anpo, M., and Che, M. (2000). Evidence of three kinds of tetrahedral vanadium (V) species in vsiβ zeolite by diffuse reflectance UV-visible and photoluminescence spectroscopies. *J. Phys. Chem. B* 104, 6012–6020. doi: 10.1021/jp0000331

Eagan, R. J., and Swearekgen, J. C. (1978). Effect of composition on the mechanical properties of aluminosilicate and borosilicate glasses. *J. Am. Ceramic Soc.* 61, 27–30. doi: 10.1111/j.1151-2916.1978.tb09222.x

Farah, H. (2008). Optical basicity analysis of vanadium-bearing silicate glasses/melts. *J. Am. Ceramic Soc.* 91, 3915–3919. doi: 10.1111/j.1551-2916.2008.02771.x

Farah, H., and Brungs, M. (2003). Oxidation-reduction equilibria of vanadium in CaO-SiO2, CaO-Al2O3-SiO2 and CaO-MgO-SiO2 melts. *J. Mater. Sci.* 38, 1885–1894. doi: 10.1023/A:1023588010572

Gao, G., Meszaros, R., Peng, M., and Wondraczek, L. (2011). Broadband UV-to-green photoconversion in V-doped lithium zinc silicate glasses and glass ceramics. *Opt. Express* 19:A312. doi: 10.1364/OE.19.00A312

Giuli, G., Paris, E., Mungall, J., Romano, C., and Dingwell, D. (2004). V oxidation state and coordination number in silicate glasses by XAS. *Am. Mineral.* 89, 1640–1646. doi: 10.2138/am-2004-11-1208

Grammes, T., Limbach, R., Bruns, S., van Wüllen, L., de Ligny, D., Kamitsos, E. I., et al. (2020). Tailoring the mechanical properties of metaluminous aluminosilicate glasses by phosphate incorporation. *Front. Mater.* 7:115. doi: 10.3389/fmats.2020.00115

Hamnabard, Z., Khalkhali, Z., Qazvini, S. S. A., Baghshahi, S., and Maghsoudipour, A. (2012). Preparation, heat treatment and photoluminescence properties of V-doped ZnOSiO 2B 2O 3 glasses. *J. Lumin* 132, 1126–1132. doi: 10.1016/j.jlumin.2011.12.083

Hensler, J. R., and Lell, E. (1969). "Ultraviolet absorption in silicate glasses," in *Frontiers in Glass Science and Technology, Proceedings Annual Meeting International Commission on Glass*, eds S. Bateson and A. G. Sadler (Toronto, ON), 51–57.

Hrubý, A. (1972). Evaluation of glass-forming tendency by means of DTA. *Czechoslovak J. Phys.* 22, 1187–1193. doi: 10.1007/BF01690134

Inaba, S., Todaka, S., Ohta, Y., and Morinaga, K. (2000). Equation for estimating the Young's modulus, shear modulus and Vickers hardness of aluminosilicate glasses. *Nippon Kinzoku Gakkaishi J. Japan Institute Metals* 64, 177–183. doi: 10.2320/jinstmet1952.64.3_177

Johnston, W. D. (1965a). Optical spectra of the various valence states of vanadium in Na2 O.2SiO2 glass. *J. Am. Ceramic Soc.* 48, 608–611. doi: 10.1111/j.1151-2916.1965.tb14688.x

Johnston, W. D. (1965b). Oxidation-reduction equilibria in molten Na2O.2SiO2 glass. *J. Am. Ceramic Soc.* 48, 184–190. doi: 10.1111/j.1151-2916.1965.tb14709.x

Khater, G. A. (2010). Glass-ceramics in the CaO–MgO–Al2O3–SiO2 system based on industrial waste materials. *J. Non Cryst. Solids* 356, 3066–3070. doi: 10.1016/j.jnoncrysol.2010.02.030

Kieffer, J. (2015). "Brillouin light scattering," in *Modern Glass Characterization.* (Hoboken, NJ: John Wiley & Sons, Inc), 1–51 doi: 10.1002/9781119051862.ch4

Kniec, K., and Marciniak, L. (2019). Different strategies of stabilization of vanadium oxidation states in Lagao3 nanocrystals. *Front. Chem.* 7:520. doi: 10.3389/fchem.2019.00520

Kornatowski, J., Sychev, M., Kuzenkov, S., Strnadová, K., Pilz, W., Kassner, D., et al. (1995). V-Ti and V-AI silicate molecular sieves of MFI topology: synthesis and characteristics. *J. Chem. Soc. Faraday Trans.* 91, 2217–2227. doi: 10.1039/FT9959102217

Laorodphan, N., Pooddee, P., Kidkhunthod, P., Kunthadee, P., Tapala, W., and Puntharod, R. (2016). Boron and pentavalent vanadium local environments in binary vanadium borate glasses. *J. Non Cryst. Solids* 453, 118–124. doi: 10.1016/j.jnoncrysol.2016.10.005

Lebouteiller, A., and Courtine, P. (1998). Improvement of a bulk optical basicity table for oxidic systems. *J. Solid State Chem.* 137, 94–103. doi: 10.1006/jssc.1997.7722

Leister, M., Ehrt, D., von der Gönna, G., Rüssel, C., and Breitbarth, F. W. (1999). Redox states and coordination of vanadium in sodium silicates melted at high temperatures. *Phys. Chem. Glasses* 40, 319–325.

Lin, C. C., and Liu, L. G. (2006). Composition dependence of elasticity in aluminosilicate glasses. *Phys. Chem. Miner.* 33, 332–346. doi: 10.1007/s00269-006-0084-z

Makishima, A., and Mackenzie, J. D. (1973). Direct calculation of Young's moidulus of glass. *J. Non Cryst. Solids* 12, 35–45. doi: 10.1016/0022-3093(73)90053-7

McKeown, D. A., Galeener, F. L., and Brown, G. E. (1984). Raman studies of Al coordination in silica-rich sodium aluminosilicate glasses and some related minerals. *J. Non Cryst. Solids* 68, 361–378. doi: 10.1016/0022-3093(84)90017-6

Moretti, R. (2005). Polymerisation, basicity, oxidation state and their role in ionic modelling of silicate melts. *Ann Geophys.* 48, 583–608. doi: 10.4401/ag-3221

Mysen, B. O. (1992). Iron and phosphorus in calcium silicate quenched melts. *Chem. Geol.* 98, 175–202. doi: 10.1016/0009-2541(92)90184-7

Mysen, B. O., and Richet, P. (2005). *Silicate Glasses and Melts : Properties and Structure*, 1st edn. Berlin: Springer.

Mysen, B. O., Virgo, D., and Scarfe, C. M. (1979). Viscosity of silicate melts as a function of pressure: structural interpretation. *Carnegie Inst Washington Yearbook* 78, 551–556.

Nascimento, M. L. F., Souza, L. A., Ferreira, E. B., and Zanotto, E. D. (2005). Can glass stability parameters infer glass forming ability? *J. Non Cryst. Solids* 351, 3296–3308. doi: 10.1016/j.jnoncrysol.2005.08.013

Neuville, D. R., and Mysen, B. O. (1996). Role of aluminium in the silicate network: *in situ*, high-temperature study of glasses and melts on the join SiO2-NaAlO2. *Geochim. Cosmochim. Acta* 60, 1727–1737. doi: 10.1016/0016-7037(96)00049-X

Ori, G., Montorsi, M., Pedone, A., and Siligardi, C. (2011). Insight into the structure of vanadium containing glasses: a molecular dynamics study. *J. Non-Crystalline Solids* 357:2571–2579. doi: 10.1016/j.jnoncrysol.2011.02.002

Pönitzsch, A., Nofz, M., Wondraczek, L., and Deubener, J. (2016). Bulk elastic properties, hardness and fatigue of calcium aluminosilicate glasses in the intermediate-silica range. *J. Non Cryst. Solids* 434, 1–12. doi: 10.1016/j.jnoncrysol.2015.12.002

Schraml-Marth, M., Wokaun, A., Pohl, M., and Krauss, H. L. (1991). Spectroscopic investigation of the structure of silica-supported vanadium oxide catalysts at submonolayer coverages. *J. Chem. Soci. Faraday Trans.* 87, 2635–2646. doi: 10.1039/ft9918702635

Schreiber, H. D. (1986). Redox processes in glass-forming melts. *J. Non Cryst. Solids* 84, 129–141. doi: 10.1016/0022-3093(86)90770-2

Shelby, J. E. (1985). Formation and properties of calcium aluminosilicate glasses. *J. Am. Ceramic Soc.* 68, 155–158. doi: 10.1111/j.1151-2916.1985.tb09656.x

Sonneville, C., De Ligny, D., Mermet, A., Champagnon, B., Martinet, C., Henderson, G. H., et al. (2013). *In situ* Brillouin study of sodium alumino silicate glasses under pressure. *J. Chem. Phys.* 139:074501. doi: 10.1063/1.4818335

Toplis, M. J., and Dingwell, D. B. (1996). The variable influence of P2O5 on the viscosity of melts of differing alkali/aluminium ratio: implications for the structural role of phosphorus in silicate melts. *Geochim. Cosmochim. Acta* 60, 4107–4121. doi: 10.1016/S0016-7037(96)00225-6

Toya, T., Tamura, Y., Kameshima, Y., and Okada, K. (2004). Preparation and properties of CaO–MgO–Al2O3–SiO2 glass-ceramics from kaolin clay refining waste (Kira) and dolomite. *Ceramics Int.* 30, 983–989. doi: 10.1016/j.ceramint.2003.11.005

Veber, A., Cicconi, M. R., Reinfelder, H., and de Ligny, D. (2018). Combined differential scanning calorimetry, raman and brillouin spectroscopies: a multiscale approach for materials investigation. *Anal. Chim. Acta* 998, 37–44. doi: 10.1016/j.aca.2017.09.045

Weigel, C., Le Losq, C., Vialla, R., Dupas, C., Clément, S., Neuville, D. R., et al. (2016). Elastic moduli of XAlSiO4 aluminosilicate glasses: effects of charge-balancing cations. *J. Non Cryst. Solids* 447, 267–272. doi: 10.1016/j.jnoncrysol.2016.06.023

Xiang, Y., Du, J., Smedskjaer, M. M., and Mauro, J. C. (2013). Structure and properties of sodium aluminosilicate glasses from molecular dynamics simulations. *J. Chem. Phys.* 139:044507. doi: 10.1063/1.4816378

Zeidler, A., Salmon, P. S., and Skinner, L. B. (2014). Packing and the structural transformations in liquid and amorphous oxides from ambient to extreme conditions. *Proc. Natl. Acad. Sci. U.S.A.* 111, 10045–10048. doi: 10.1073/pnas.1405660111

Conflict of Interest: The authors declare that the research was conducted in the absence of any commercial or financial relationships that could be construed as a potential conflict of interest.